分 类 号_____ 学号_____D201277241_____

学校代码__10487__ 密级_____

華中科技大學

博 士 学 位 论 文

太阳能光热梯级发电系统建模及其特性研究

学位申请人：张成

学 科 专 业：热能工程

指 导 教 师：高伟 教授

Inmaculada Arauzo 教授

张燕平 副教授

答 辩 日 期：2018 年 1 月 20 日

A Thesis Submitted in Partial Fulfillment of the
Requirements for the Ph.D

Cascade solar thermal power system modeling and research of the key features

Student : Cheng Zhang

Major : Thermal Engineering

Supervisor : Prof. Wei Gao

Prof. Inmaculada Arauzo

Associate Prof. Yanping Zhang

Huazhong University of Science & Technology

Wuhan 430074, P. R. China

January 20, 2018

独创性声明

本人声明所呈交的学位论文是我个人在导师的指导下进行的研究工作及取得的研究成果。尽我所知，除文中已标明引用的内容外，本论文不包含任何其他人或集体已经发表或撰写过的研究成果。对本文的研究做出贡献的个人和集体，均已在文中以明确方式标明。本人完全意识到本声明的法律结果由本人承担。

学位论文作者签名：

日期：　　年　　月　　日

学位论文版权使用授权书

本学位论文作者完全了解学校有关保留、使用学位论文的规定，即：学校有权保留并向国家有关部门或机构送交论文的复印件和电子版，允许论文被查阅和借阅。本人授权华中科技大学可以将本学位论文的全部或部分内容编入有关数据库进行检索，可以采用影印、缩印或扫描等复制手段保存和汇编本学位论文。

本论文属于　保密 □，在 ____ 年解密后适用本授权书。

　　不保密 □。

（请在以上方框内打“√”）

学位论文作者签名：　　指导教师签名：

日期：　　年　　月　　日　　日期：　　年　　月　　日

摘　要

随着化石能源消耗和环境污染问题的凸显，太阳能被广泛认为是未来最有潜力替代传统化石能源的清洁能源。本文以国家国际合作项目专项“太阳能梯级集热发电系统关键技术合作研究”为背景，目标是研究太阳能光热发电装置，利用各种传统型式的太阳能光热发电系统的优缺点以及热力特性，提出并组建、优化太阳能梯级集热发电系统，为探索出大规模低成本高效率利用太阳能的光热发电技术提供新的方案。主要研究内容包括：

提出了多种采用梯级集热和梯级发电的太阳能光热梯级发电系统。在梯级系统中，采用了多种型式的集热器，实现能量的梯级收集，采用多种形式的热力循环，实现能量的梯级利用。经过系统评估、参数选取、初步计算、方案比较，确定了两种具有代表性的梯级系统方案。

采用数学计算工具和系统开发工具，建立了梯级系统中各部件的机理模型，进而组建了梯级系统。采用面向对象的方法，充分利用了继承、多态等特性，保证了各部件之间既具有独立性又具有关联性。其中，斯特林机的建模过程中，考虑了多种不可逆过程及多类损失，建立了较为完善的斯特林机机理模型，并进行了模型验证分析。结果表明，所建立的斯特林机模型的精度要高于传统的经典斯特林机模型。

研究了太阳能光热梯级发电系统中斯特林机组不同排布方式对系统效率的影响。通过分析斯特林机组的各种不同的排布方式，发现串联连接是最佳的连接型式，斯特林机组具有最佳健壮性和最大的发电效率，梯级发电系统也具有最大的光热发电效率。

提出了分阶段加热的方法，有效降低了蒸汽发生系统中的㶲损。在传统蒸汽发生系统的换热过程中，加热流体无相变，被加热流体有相变，两者存在较大的换热温差，换热过程有较大的㶲损。本文提出分阶段加热的方法，通过改变加热流体的流量，减小换热温差，降低换热过程的㶲损。

提出了太阳能光热梯级发电系统与传统型式太阳能光热发电系统的对比方法。本文针对新型梯级发电系统提出了其与传统型式太阳能光热发电独立系统的对比方法。梯级系统在一定的参数条件下，相比其对应的独立系统，具有更高的总体光电转换效率。

建立了太阳能集热发电试验平台，并开展了相关的试验工作。在相关试验条件下，槽式集热器的热效率在 60.1% 到 62.8% 之间，槽式集热器的热效率在 39.7% 到 63.3% 之间。试验还验证了建立的槽式集热器和碟式集热器模型。

关键词： 槽式集热器,碟式集热器,朗肯循环,斯特林循环,斯特林机组,梯级发电

Abstract

With the increasing awareness of the problem of fossil energy consumption and environmental pollution, solar energy is regarded as the best potential alternative of fossil energy. This research is based on the national cooperation project "Collaborative research on key technologies to produce electricity by cascade utilization solar thermal energy". The objective of this project is to conduct research on the equipment of solar thermal power generation system, to propose, develop and optimize a solar thermal cascade system depending on the advantages and disadvantages of the solar thermal power generation technologies, and to explore a new feasible technology for large-scale solar thermal power generation. The main contents and conclusions of this thesis are as follows:

Multiple topological structures with cascade collection and cascade utilization of the cascade systems were proposed. In these systems, different types of collectors were used for cascade collection and different types of thermodynamic cycles were used for cascade utilization. After system evaluation, parameter selection, preliminary calculation and scheme comparison, two representative typical schemes were selected.

Mechanism models were established for the components of solar thermal power generation system by using mathematical calculation tool and system development tool. The modeling process uses an object-oriented approach, taking full advantage of inheritance, polymorphism and other characteristics, to ensure each component has both independence and relevance. Among them, the Stirling machine modeling process, considering various irreversibilities and losses, established a more accurate Stirling mechanism model with verification analysis. The results show that the accuracy of the established Stirling model is higher than that of the classical classical Stirling engine models.

The effect of different arrangements of Stirling engines on the efficiency of the cascade system was studied. Through the analysis of different arrangements of Stirling engines, it was found that series connection is the best connection type for the best robustness and maximum efficiency of the Stirling engines, and the largest solar-to-electric efficiency of the cascade system.

A method of multistage heating was proposed, which can effectively reduce the exergy loss of steam generating system. During the entire heat exchange process of a conventional steam generating system, there is no phase change in the heating fluid and there is a phase

change in the heated fluid. There exist large heat transfer temperature differences between the two fluids in the heat exchangers, which makes large entropy production during the heat exchange process. In this thesis, a method of heating in stages is proposed, in which the flow rates of the heating fluid in different heat exchangers are controlled to reduce the heat transfer temperature difference and the exergy losses.

A comparison method of cascade system and traditional solar thermal power generation systems is proposed. In this thesis, corresponding independent systems of the cascade system was proposed for comparison. It is found that the cascade system has a higher overall solar-to-electric conversion efficiency under certain parameters compared to its corresponding independent systems.

A solar thermal power generation test platform was established, and the relevant experimental work was carried out. Under the relevant test conditions, the thermal efficiency of trough collectors is between 60.1% and 62.8%, and that of trough collectors is between 39.7% and 63.3%. The experiment also validated the established trough collector and dish collector models.

Key words: parabolic trough collector, parabolic dish collector, Rankine cycle, Stirling cycle, Stirling engine array, cascade solar thermal power

目　录

插图索引

表格索引

一　建模

为了研究所提出的梯级系统的性能，使用 EES（Engineering Equation Solver）和 MATLAB（Matrix Laboratory）作为计算工具和开发工具开发了系统的机理模型。系统建模采用自底向上的设计方法。首先，在 EES 中建立机理模型用于来验证模型中各参数间的物理关系。其次，使用面向对象的方法在 MATLAB 中开发出组件模型，它充分利用了面向对象的继承性和多态性来保证组件之间的独立性和相关性。依据不同流体，创建了三个回路（空气回路，水回路和油回路），并确定了一些关键部件的特定的状态参数。依据这些关键部件的热力学特性和热力学第二定律，为其创建了基于能量平衡的机理模型。

以下部分介绍一些关键部件的模型。

1.1　部件建模

1.1.1　槽式集热器

槽式集热器由反射镜和接收器组成。反射镜（镜面）反射太阳直射辐射并将其会聚到位于抛物槽面焦线处的接收器上。接收器通常包含涂有高吸收率涂层的金属吸热管。在吸热管外部设有玻璃管以减少散热损失，吸热管和玻璃管之间通常被抽成真空以进一步减少热损。

在反射过程中存在着光学损失，主要包含以下几项[3]：

- 遮挡损失
- 追踪损失
- 形状损失
- 反射率损失
- 镜面沾污损失
- 其它未列入损失

还有一项，即太阳直射的阳光与集热器开口不垂直时，应该考虑入射角带来的损失 $K(\theta)$（也称为余弦损失）。该损失是太阳入射角与集热器开口法线交角（θ）的函数。

桑迪亚国家实验室的 Dudley 等[4] 通过试验研究给出了槽式集热器的余弦损失计

算公式:

$$K(\theta) = \cos\theta + 0.000884\theta - 0.00005369\theta^2 \tag{1.1}$$

图1-1给出了槽式集热器反射太阳光线的示意图, 图中还标出了影响光学损失的一些参数。整个光学损失与下列五个参数有关:

(1) 反射率, ρ: 只有一部分入射辐射会反射到接收器上。这一部分由反射镜的种类决定。对于清洗干净的商业槽式反射镜, 其反射率可以假定为 0.9。

(2) 拦截因子, γ: 由于反射镜的微观缺陷或抛物面槽式集热器的宏观形状误差, 反射镜反射的太阳直射辐射中的一部分不能到达吸热管(例如组装不精确)。这些缺陷或误差导致一些光线以错误的角度反射, 因此它们不能被吸热管拦截吸收。这些损失通过称为拦截因子的光学参数来量化。对于正确组装的集热器而言, 该参数通常为 0.95。

(3) 透射率 τ: 到达接收器的玻璃管的太阳直射辐射只有一部分能够透射它。透射玻璃管的辐射与投射到其上的总的入射辐射之间的比称为透射率 τ, 它通常取为 0.93。

(4) 吸热管涂层的吸收率, α_{abs}: 该参数量化了吸热管吸收的能量与到达吸热管外壁的总辐射量的比例。对于有陶瓷涂层的金属吸热管, 该参数通常为 0.95, 而对于涂有黑色镍或铬的吸热管, 该参数值稍低。

(5) 沾污因子, F_e: 反射镜上的污垢会降低反射率, 因此需要考虑沾污带来的影响。沾污因子 F_e 的引入考虑了反射镜和玻璃管在清洗干净之后的逐渐产生的沾污。

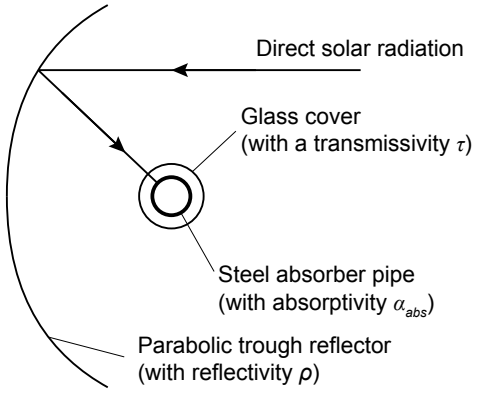

图 1-1　槽式集热器结构示意图

穿透玻璃管到达吸热器的能量可以表示为

$$P = I_r w_{tc} L_{tc} \rho \gamma \tau F_e K(\theta) \tag{1.2}$$

为了简化吸热器的吸热过程,通常将其视为均匀的热流量 q''。

$$q'' = \frac{P}{\pi d_o L_{tc}} = \frac{I_r w_{tc} \rho \gamma \tau F_e K(\theta)}{\pi d_o} \tag{1.3}$$

假设整体传热系数 $U(T_{abs})$ 沿着整个集热器的长度方向是均匀的,这样就可以利用附录B中的传热计算公式。吸收管的传热分析示意图如图1-2所示。

$$\frac{T_o - T_{amb} - \dfrac{q''}{U(T_{abs})}}{T_i - T_{amb} - \dfrac{q''}{U(T_{abs})}} = \exp(-\frac{U(T_{abs})\pi d_o L_{tc}}{\dot{m} c_p}) \tag{1.4}$$

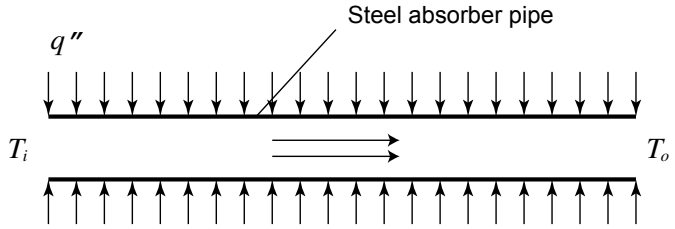

图 1-2　吸热管的传热分析示意图

由于管道中的努塞尔数 Nu 非常大(大约为 $1/times10^4$),吸热管和导热油之间存在很小的温差。所以平均流体温度 $(T_i + T_o)/2$ 可以用作 T_{abs} 的平均值,$U(T_{abs})$ 可以用 Romero 和 Zarza 给出的二阶多项式函数表示[5]。达到所需加热效果的槽式集热器的长度 L_{tc} 可以从公式(1.4)中获得。

垂直投射到槽式集热器开口的能量为

$$Q_{total} = I_r L_{tc} w_{tc} \tag{1.5}$$

被传热流体吸收的能量为

$$Q_{use} = \dot{m} c_p (T_o - T_i) \tag{1.6}$$

槽式集热器的集热效率为

$$\eta_{tc} = \frac{Q_{use}}{Q_{total}} = \frac{I_r L_{tc} w_{tc}}{\dot{m} c_p (T_o - T_i)} \tag{1.7}$$

1.1.2 碟式集热器

碟式集热器由发射镜和接收器组成。反射镜通过追踪太阳来将太阳光反射并会聚到位于反射镜焦点处的接收器熵。碟式集热器需要采用双轴跟踪系统来不间断地追踪太阳的轨迹。

碟式集热器的追踪系统主要有两种型式:[6]

- 由方位传感器进行的方位高度角跟踪,或由计算得到的太阳坐标通过控制系统进行控制。
- 极轴跟踪,集热器围绕与地轴平行的轴旋转追踪太阳。

在传统的碟式斯特林机系统中,斯特林发动机放置在碟式集热器的焦点上。斯特林机设有接收器来吸收会聚的阳光。接收器由一个开孔和一个吸热器组成。斯特林接收器的开孔位于反射器的焦点处,以减少辐射和对流损失。吸热器吸收太阳辐射能并将产生的热能传递给斯特林机的工作气体,为斯特林循环提供热量,使斯特林机的曲轴连续往复运动。直接连接到斯特林机曲轴的发电机将机械能转化为电能。

本文提出的梯级系统中,碟式集热器的焦点处放置有容积式接收器。一个金属螺旋管(称为吸热管)作为吸热器位于接收器中以吸收集中的太阳能。空气(或氮气)被用作传热流体流经吸热管以传输被吸热管吸收的能量,为斯特林机提供热源。

碟式反射镜是碟式系统的重要元件。弯曲的反射表面可以利用单独的小平面连接起来形成,或是通过由连续气室成形的拉伸膜来实现。在所有的情况下,曲面都应涂铝或银以提高反射率。

本文选用 SES(Stirling Energy System)公司生产的碟式反射镜作为梯级集热系统的碟式反射镜,其主要参数见于表1.1。碟式接收器为自行设计研制的接收器,图1-3是其结构示意图。

碟形接收器模型涉及的损失包括:接收器拦截损失,由于阴影造成的损失以及热损失。热损失占所有这些损失的最大部分,这部分损失由传导,对流和辐射三种形式组成。为了详细分析碟式接收器的热损失,建立了如图1-4所示的热网络模型。该网络模型考虑了以下损失:

- 由接收器孔腔从接收器开口反射出去的辐射能损失,$q_{rad,ref}$。
- 由于和接收器的绝热层发生热传导产生的损失,$q_{cond,tot}$。
- 无风的条件下接收器开口处发生的自然对流损失,$q_{conv,free}$。
- 有风的条件下接收器开口处发生的强制对流损失,$q_{conv,forc}$。
- 由接收器孔腔发射出去的热辐射造成的辐射损失,$q_{rad,emit}$。

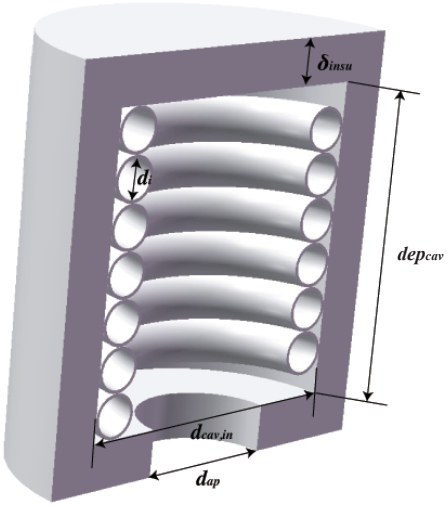

图 1-3　碟式接收器的结构示意图

表 1.1　碟式集热器的主要参数

Parameter	Value	Parameter	Value	Parameter	Value
d_{cav}	0.46 m	ϵ_{insu}	0.6	θ_{dc}	45°
δ_{insu}	0.075 m	α_{cav}	0.87	γ	0.97
dep_{cav}	0.23 m	δ_a	0.005 m	$\eta_{shading}$	0.95
d_{ap}	0.184 m	$d_{i,1}$	0.07 m	ρ	0.91
λ_{insu}	0.06 W/(m · K)	A_{dc}	87.7 m^2		

为了求解图1-4中的热网络结构图, 必须仔细分析图中各热流量的关系和求解方程。

(1) 入射到接收器的能量, q_i

为了简化模型, 不考虑接收器对反射镜造成的遮挡, 以及太阳跟踪系统的调节滞后造成的不利影响。

$$q_i = I_r A_{dc} \gamma \eta_{shading} \rho \tag{1.8}$$

In Equation (1.8), γ is the intercept factor, $\eta_{shading}$ is the shading factor between different collectors, ρ is the reflectivity of the reflector. 在方程 (1.8) 中, γ 是拦截因子,

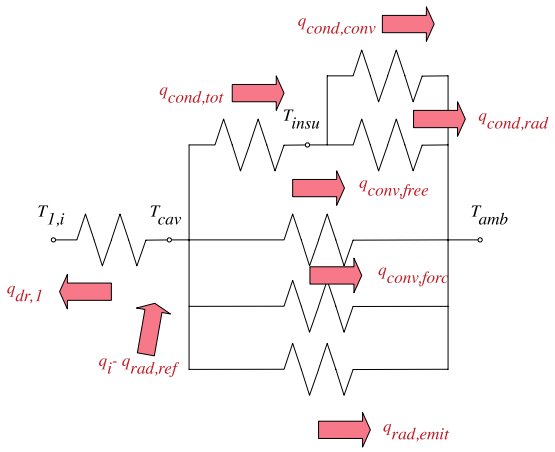

图 1-4　碟式接收器的热网络模型

$\eta_{shading}$ 是不同集热器之间遮挡造成的遮挡因子，ρ 是反射镜的反射率。

(2) 传热流体与吸热管之间的换热，$q_{dr,1}$

传热流体于吸热管之间的换热简化为经典的流体流过等壁温管道的换热模型。这样，$q_{dr,1}$ 可以由下式得到

$$q_{dr,1} = h_{dr,1} A_{dr,1} \Delta T_{ln,dr,1} \tag{1.9}$$

where

$$h_{dr,1} = Nu_{tube} \lambda_{dr,1} / d_{i,1} \tag{1.10}$$

$$Nu_{tube} = c_r Nu'_{tube} \tag{1.11}$$

该式为修正后应用于螺旋管的努赛尔数计算公式，式中存在基于弯管曲率的螺旋因子 c_r 作为修正系数。c_r 的表达式为：[7]

$$c_r = 1 + 3.5 \frac{d_{i,1}}{d_{cav} - d_{i,1} - 2\delta_a} \tag{1.12}$$

Nu'_{tube} 是直圆管的努赛尔数，它由下式计算：[8]

$$Nu'_{tube} = 0.027 Re_{tube}^{0.8} Pr_{tube}^{1/3} (\mu_{tube} / \mu_{tube,w})^{0.14} \tag{1.13}$$

传热流体与管壁之间的对数温差 $\Delta T_{ln,dr,1}$ 可以写作

$$\Delta T_{ln,dr,1} = \frac{(T_{cav} - T_{dc,i}) - (T_{cav} - T_{dc,o})}{\ln \dfrac{T_{cav} - T_{dc,i}}{T_{cav} - T_{dc,o}}} \tag{1.14}$$

(3) 由接收器内壁从接收器开口反射出去的辐射能损失, $q_{rad,ref}$

$$q_{rad,ref} = (1 - \alpha_{eff}) q_i \tag{1.15}$$

其中, α_{eff} 是接收器的等效吸收率, 它由下式算得:

$$\alpha_{eff} = \frac{\alpha_{cav}}{\alpha_{cav} + (1 - \alpha_{cav}) \dfrac{A_{ap}}{A_{cav}}} \tag{1.16}$$

α_{cav} 是接收器孔腔材料的吸收率, A_{cav} 是孔腔的总面积, A_{ap} 是开口面积.

(4) 由于和接收器的绝热层发生热传导产生的损失, $q_{cond,tot}$

$$q_{cond,tot} = 2\pi \lambda_{insu} dep_{cav} \frac{T_{cav} - T_{insu}}{\ln(1 + 2\delta_{insu}/d_{cav})} \tag{1.17}$$

其中, T_{cav} 是孔腔的内壁温度, T_{insu} 是绝热层的外壁温度。

(5) *Convection losses from the receiver insulating layer,* $q_{cond,conv}$

$$q_{cond,conv} = h_{insu} A_{insu} (T_{insu} - T_{amb}) = \frac{k_{insu} Nu_{insu} A_{insu} (T_{insu} - T_{amb})}{d_{cav} + 2\delta_{insu}} \tag{1.18}$$

where Nu_{insu} can be obtained from the correlation for flow over a circular cylinder.[9]

(6) *Radiation losses from the receiver insulating layer,* $q_{cond,rad}$

$$q_{cond,rad} = \epsilon_{insu} A_{insu} \sigma (T_{insu}^4 - T_{amb}^4) \tag{1.19}$$

(7) *Free convection from the cavity in the absence of wind,* $q_{conv,free}$

Ma[10] conducted tests to determine the free convection losses from the receiver for alternative setups, and the data were consistent with Stine and McDonald's free convection correlation. It is assumed that forced convection is independent of free convection in the receiver, so the total convection losses can be represented as the total of the free and forced convection losses as shown in Figure 1-4.

$$q_{conv,free} = h_{free} A_{cav} (T_{cav} - T_{amb}) \tag{1.20}$$

where $h_{free} = k_{film} Nu_{free} / \overline{d_{cav}}$, $\overline{d_{cav}}$ is the effective diameter of the cavity, $\overline{d_{cav}} = d_{cav} - 2d_i - 4\delta_a$. d_i =0.066 m

(8) *Force convection from the cavity in the presence of wind,* $q_{conv,forc}$

$$q_{conv,forc} = h_{forc} A_{cav} (T_{cav} - T_{amb}) \tag{1.21}$$

Wu et al.[11] present a comprehensive review and systematic summarization of convection heat loss from cavity receiver in parabolic dish solar thermal power system. And we choose the correlation presented by Leibfried and Ortjohann[12]. This correlation gives an extended model of Koenig and Marvin[13] and Stine and Diver[14] with better results.

For forced convection loss, side-on wind convection loss model given by Ma[10], which is independent of the aperture orientation, is used

$$h_{forc} = 0.1967 v_{wind}^{1.849} \tag{1.22}$$

(9) *Emission losses due to thermal radiation emitted from the receiver aperture,* $q_{rad,emit}$

The emissivity is set equal to the effective absorptivity of the cavity (gray body),

$$\epsilon_{cav} = \alpha_{eff} \tag{1.23}$$

$$q_{rad,emit} = \epsilon_{cav} A_{ap} \sigma (T_{cav}^4 - T_{amb}^4) \tag{1.24}$$

From Figure 1-4, it can be found that

$$q_{eff} = q_i - q_{rad,ref} \tag{1.25}$$

$$q_{eff} = q_{dr,1} + q_{cond,tot} + q_{conv,free} + q_{conv,forc} + q_{rad,emit} \tag{1.26}$$

$$q_{cond,tot} = q_{cond,conv} + q_{cond,rad} \tag{1.27}$$

So the temperature nodes in the thermal network can be solved by these equations. $q_{dr,1}$ can be obtained from Equation (1.9), and efficiency of the dish receiver

$$\eta_{dr} = \frac{q_{dr,1}}{q_i} \tag{1.28}$$

Efficiency of the dish collector

$$\eta_{dc} = \frac{q_{dr,1}}{I_r A_{dc}} \tag{1.29}$$

1.1.3 Stirling engine

1.1.3.1 Theoretical Stirling cycle

In a Stirling cycle, there are two isothermal processes that exchange heat with heating and cooling fluids, two isochoric processes that exchange heat with regenerator. Figure 1-5 shows the T-s diagram of a typical Stirling cycle. The heat absorbed by regenerator in process 4-1 is reused in process 2-3, but only able to heat the working gas from 2 to 3' due to the imperfect regeneration. e is defined as the regenerator effectiveness[15,16], $e = \dfrac{T_R - T_L}{T_H - T_L}$, where T_H is the temperature in the hot space, T_L is the temperature in the cold space, T_R is the effective working fluid temperature in the regenerator.

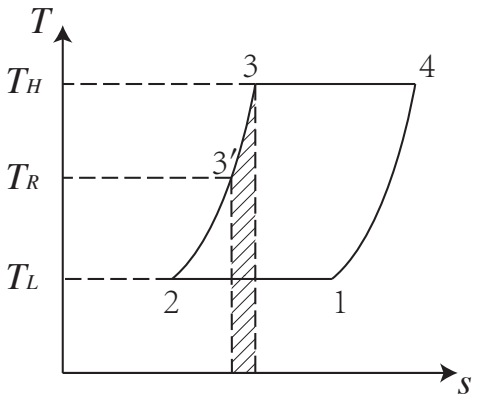

图 1-5 T-s diagram of a Stirling cycle

In order to obtain a simplified analytical model, several simplifications are made:

- The working gas in Stirling engines obeys the idea gas law.
- No heat loss to the environment for Stirling engines.
- Overall heat transfer coefficients of the fluids are constant.
- A symmetrical regenerator behavior is assumed so that a simple effectiveness can be obtain by $T_R = \dfrac{T_H - T_L}{\ln(T_H/T_L)}$.[15,16]

To consider internal irreversibilities in a Stirling cycle made by dead volumes, total dead volume V_D can be divided into heater dead volume V_{DH}, regenerator dead volume V_{DR} and cooler dead volume V_{DC}.[17], There exists a factor K to describe the dead volumes

under different temperatures. K is relevant with temperatures in the process and regenerator effectiveness.

$$K = \frac{V_{DH}}{T_H} + \frac{V_{DR}}{T_R} + \frac{V_{DC}}{T_L} \tag{1.30}$$

For the isothermal compression process 1-2, the output work

$$W_{12} = \int_{V_E+V_C}^{V_E} p_{12} dV = -mRT_L \ln \frac{V_E + V_C + KT_L}{V_E + KT_L} \tag{1.31}$$

For the isothermal expansion process 3-4, the output work

$$W_{34} = \int_{V_E}^{V_E+V_C} p_{34} dV = mRT_H \ln \frac{V_E + V_C + KT_H}{V_E + KT_H} \tag{1.32}$$

Define $\gamma_H = \dfrac{V_E + V_C + KT_H}{V_E + KT_H}$, and $\gamma_L = \dfrac{V_E + V_C + KT_L}{V_E + KT_L}$. In a cycle, the theoretical output work

$$W_{th} = W_{12} + W_{34} = mR(T_H \ln \gamma_H - T_L \ln \gamma_L) \tag{1.33}$$

For the isochoric heating process 3'-3, the absorbed heat

$$Q_{3'3} = nc_v(T_H - T_R) = \frac{1-e}{k-1} mR(T_H - T_L) \tag{1.35}$$

For the the isothermal expansion process 3-4, the absorbed heat

$$Q_{34} = W_{34} = mRT_H \ln \gamma_H \tag{1.36}$$

In a cycle, the theoretical absorbed heat

$$Q_{th} = Q_{3'3} + Q_{34} = \frac{1-e}{k-1} mR(T_H - T_L) + mRT_H \ln \gamma_H \tag{1.37}$$

1.1.3.2 Irrevisibilities and losses

(1) Non-ideal heat transfer effect

Because of non-ideal heater and cooler, the working fluid temperature (T_H/T_L) in these two heat exchangers is less/higher than the wall temperature (T_{hw}/T_{cw}), respectively. T_H and T_L can be corrected by the wall temperatures as follows:

$$T_H = T_{hw} - \frac{Qs_{se}}{h_h A_{hw}} \tag{1.38}$$

$$T_L = T_{cw} + \frac{(Q-W)s_{se}}{h_c A_{cw}} \tag{1.39}$$

The heat transfer coefficient can be obtained using the following correlation[1]:

$$h_{h,c} = \frac{\mu c_p f_{Re}}{2D_{h,c} Pr_{h,c}} \tag{1.40}$$

where f_{Re} is a Reynolds friction factor defined as:

$$f_{Re} = 0.0791 Re_{h,c}^{0.75} \tag{1.41}$$

$Re_{h,c}$, $Pr_{h,c}$ and $D_{h,c}$ are Reynolds number, Prandtl number and hydraulic diameter of the heater/cooler exchanger.

(2) Effect of pressure drop

Pressure drops in the heat exchangers cause power losses of the Stirling engine. The pressure drops can be expressed by:[18]

$$\Delta p = -\frac{2 f_{Re} \mu u V}{d^2 A} \tag{1.42}$$

where u is the working gas speed, V is volume, A is flow cross-section area.

The net power loss of the Stirling engine due to pressure drop of the heat exchangers can be evaluated by:

$$W_{pd} = \oint \sum_{i=E,C} (\Delta p_i \frac{dV_i}{d\theta}) d\theta \tag{1.43}$$

(3) Effect of finite speed of piston and mechanical friction

Due to the finite speed of piston, the pressure on the piston surface is different from the pressure of expansion and compression spaces. It has been demonstrated that the pressure on the piston surface in the expansion process is less than the mean pressure

in the expansion space. Similarly, the pressure on the piston surface in the compression process is greater than the mean pressure in the compression space. This means the output work is less than the theoretical value. Besides, The output work also reduces due to mechanical friction. The output work loss due to finite speed of piston and mechanical friction can be obtained as follows:[1]

$$W_{fs} = \oint p(\pm\frac{au_p}{c} \pm \frac{\Delta p_f}{p})dV \tag{1.44}$$

where the sign $(+)$ is used in the compression space, and the sign $(-)$ is used in the expansion space. p is the mean pressure in the compression/expansion space, u_p is velocity of the piston, c is the average speed of molecules and Δp_f is the pressure loss due to mechanical friction. Δp_f, a and c can be expressed by:[19]

$$\Delta p_f = 0.97 + 0.009 s_{se} \tag{1.45}$$

$$a = \sqrt{3k} \tag{1.46}$$

$$c = \sqrt{3RT} \tag{1.47}$$

(4) Energy losses due to internal conduction

The temperature differs from the heater and cooler, heat losses from heater to cooler exists due to internal conduction through the walls of regenerator.[20] The internal conduction loss in a cycle can be expressed by follows:

$$Q_{id} = \frac{k_r A_r}{L_r s_{se}}(T_{hw} - T_{cw}) \tag{1.48}$$

where, k_r, A_r and L_r denote the regenerator matrix conductivity, regenerator length, and regenerator conductive area respectively.

(5) Energy losses due to shuttle conduction

The displacer shuttles between the expansion and compression space. It absorbs heat during the hot end of its stroke and releases it during the cold end of its stroke. This heat loss can be estimated as[21]:

$$Q_{sc} = 0.4\frac{Z^2 k_p D_p}{J L_d s_{se}}(T_H - T_L) \tag{1.49}$$

where, Z, k_p, D_p, J and L_d denote the displacer stroke, piston thermal conductivity, displacer diameter, gap between the displacer and the cylinder, and length of the displacer respectively.

So, in a Stirling engine, the total absorbed heat in a cycle

$$Q = Q_{th} + Q_{id} + Q_{sc} \tag{1.50}$$

the output work

$$W = W_{th} - W_{pd} - W_{fs} \tag{1.51}$$

Power of the Stirling engine

$$P = W s_{se} \tag{1.52}$$

Efficiency of the Stirling engine

$$\eta = W/Q \tag{1.53}$$

1.1.3.3 Model validation

Evaluation of the developed thermal model is performed by considering the GPU-3 Stirling engine as a case study. Design specifications of the GPU-3 Stirling engine are indicated in Table 1.2. The thermal efficiency and power of the proposed Stirling engine model are compared with previous thermal models and experimental data as shown in Table 1.3 and Table 1.4.

It can be found that the proposed model has much better agreement with the experimental results than previous thermal models at various rotation speeds and mean effective pressures. It is required to mention that in all thermal models both power W and input heat Q are determined by the thermal process of heat transfer between the wall and working gas. In the proposed model, W and Q are obtained from Equation (1.38) and (1.39). Therefore all the three parameters W, Q and η are determined by the thermal model and input parameters to the model. These input parameters includes heater, cooler, mean effective pressure, type of working gas and geometrical specification of the engine.

Table 1.3 and 1.4 indicate that when mean effective pressure of the engine increases from 2.76 MPa to 6.90 MPa, best performance (efficiency and power) prediction of the proposed model exists. When rotation speed increases from 16.67 Hz to 58.33 Hz, error in prediction of performance of the proposed model increases. The proposed model may have the

表 1.2　Design specifications of the GPU-3 Stirling engine[1,2]

Parameter	Value
Engine type	β
Working gas	Helium
Mass of the working gas	1.136 g
Heater	
Number of tubes	40
Tube external diameter	4.83×10^{-3} m
Tube internal diameter	3.02×10^{-3} m
Tube length (cylinder side)	0.1164 m
Tube length (regenerator side)	0.1289 m
Cooler	
Number of tubes	312
Tube external diameter	1.59×10^{-3} m
Tube internal diameter	1.09×10^{-3} m
Average tube length	4.61×10^{-2} m
Regenerator	
Number of regenerator	8
Regenerator internal diameter	2.26×10^{-2} m
Regenerator length	2.26×10^{-2} m
Diameter of regenerator tube	4×10^{-5} m
Material	Stainless steel
Volume	
Swept Vol. (expansion/compression)	120.82/114.13 cm^3
Clearance Vol. (expansion/compression)	30.52/28.68 cm^3
Dead Vol. (heater/cooler/regenerator)	70.28/13.18/50.55 cm^3

表 1.3 Thermal efficiency of the models and experimental data (at T_{hw} =922 K and T_{cw} =288 K)

Rotation speed (Hz)	Mean effective pressure (MPa)	The simple analysis (variable Pr[18])			The adiabatic analysis (simple II[20])			The proposed Stirling engine model			Experimental efficiency[1]
		Value (%)	Error (%)	Average error (%)	Value (%)	Error (%)	Average error (%)	Value (%)	Error (%)	Average error (%)	Actual value (%)
16.67	2.76	38.72	18.22	17.90	32.48	11.98	12.85	28.16	7.66	12.10	20.50
25.00		36.16	15.46		31.21	10.51		27.75	7.05		20.70
33.33		33.79	15.79		29.45	11.45		27.43	9.43		18.00
41.67		31.48	16.28		27.45	12.25		27.17	11.97		15.20
50.00		29.12	17.32		25.21	13.41		26.94	15.14		11.80
58.33		29.74	24.34		22.89	17.49		26.74	21.34		5.40
25.00	4.14	35.65	10.85	11.46	32.29	7.49	8.28	27.29	2.49	6.65	24.80
33.33		33.52	9.62		30.40	6.50		26.94	3.04		23.90
41.67		31.48	10.18		28.39	7.09		26.65	5.35		21.30
50.00		29.45	11.25		26.33	8.13		26.39	8.19		18.20
58.33		27.40	15.40		24.21	12.21		26.17	14.17		12.00
41.67	5.52	31.20	8.70	10.82	28.59	6.09	8.11	26.24	3.74	7.48	22.50
50.00		29.33	10.53		26.62	7.82		25.97	7.17		18.80
58.33		27.44	13.24		24.62	10.42		25.73	11.53		14.20
50.00	6.90	29.07	10.37	11.73	26.61	7.91	9.19	25.62	6.92	9.05	18.70
58.33		27.29	13.09		24.67	10.47		25.37	11.17		14.20

表 1.4　Output power of the models and experimental data (at T_{hw} =922 K and T_{cw} =288 K)

Rotation speed (Hz)	Mean effective pressure (MPa)	The simple analysis (variable Pr[18])			The adiabatic analysis (simple II[20])			The proposed Stirling engine model			Experiment (kW)[1]
		Value (kW)	Error (%)	Average error (%)	Value (kW)	Error (%)	Average error (%)	Value (kW)	Error (%)	Average error (%)	Actual value (kW)
16.67	2.76	1.796	119.02	272.03	1.772	116.10	254.71	0.861	4.98	104.84	0.82
25.00		2.555	128.13		2.500	123.21		1.253	11.88		1.12
33.33		3.215	165.70		3.117	157.60		1.632	34.88		1.21
41.67		3.769	211.49		3.615	198.76		2.001	65.37		1.21
50.00		4.195	303.37		3.973	282.08		2.362	127.12		1.04
58.33		4.505	704.46		4.203	650.54		2.715	384.82		0.56
25.00	4.14	3.844	114.75	259.70	3.761	110.11	158.41	1.818	1.56	39.83	1.79
33.33		4.856	120.73		4.708	114.00		2.362	7.36		2.20
41.67		5.734	136.94		5.501	127.31		2.890	19.42		2.42
50.00		6.462	174.98		6.126	160.68		3.405	44.89		2.35
58.33		7.030	306.36		6.573	279.94		3.908	125.90		1.73
41.67	5.52	7.645	133.08	180.02	7.334	123.60	164.91	3.742	14.09	43.68	3.28
50.00		8.655	163.87		8.206	150.18		4.401	34.18		3.28
58.33		9.470	243.12		8.858	220.94		5.045	82.79		2.76
50.00	6.90	10.788	174.50	287.04	10.223	160.13	263.63	5.362	36.44	97.75	3.93
58.33		11.840	399.58		11.071	367.13		6.140	159.07		2.37

best performance prediction at a low rotation speed, with mean effective pressure between 4.14 MPa and 5.52 MPa.

However, there is still some discrepancy between the the simulation results of proposed model and the experimental data. In the future researches, more accurate models of Stirling engine may be developed by considering other irreversibilities such as heat loss to the environment, gas spring hysteresis, and etc. It is worth pointing that there are more accurate Stirling engine models. For example, polytropic simulation models of Stirling engine show higher accuracy than our proposed model[1,22]. However, the model needs more costly calculations and the polytropic indexes are engine-specific.

1.1.3.4 Heat transfer between the engine and the fluids

For a Stirling engine thermal process, the wall temperatures of the heater and cooler are considered to be uniform and constant. The heat transferred between the wall and the fluids after a contact area of dA is

$$(T_w - T)UdA = \dot{m}c_p dT \tag{1.54}$$

$$\frac{dT}{T - T_w} = -\frac{UdA}{\dot{m}c_p} \tag{1.55}$$

With $T(0) = T_i$, $T(A) = T_o$,

$$\frac{T_o - T_w}{T_i - T_w} = \exp(-\frac{UA}{\dot{m}c_p}) \tag{1.56}$$

For a Stirling engine, T_{hw} or T_{cw} can be used to substitute T_w to get the relationships between $T_{i,h}$, $T_{o,h}$ and T_{hw}, or $T_{i,c}$, $T_{o,c}$ and T_{cw} respectively.

$$\frac{T_{o,h} - T_{hw}}{T_{i,h} - T_{hw}} = \exp(-\frac{U_h A_h}{\dot{m}_h c_{p,h}}) \tag{1.57}$$

$$\frac{T_{o,c} - T_{cw}}{T_{i,c} - T_{cw}} = \exp(-\frac{U_c A_c}{\dot{m}_c c_{p,c}}) \tag{1.58}$$

Heat transferred from heating fluid to Stirling engine in a cycle

$$\dot{m}_h c_{p,h}(T_{i,h} - T_{o,h})/s_{se} = Q \tag{1.59}$$

Heat transferred from Stirling engine to cooling fluid in a cycle

$$\dot{m}_c c_{p,c}(T_{o,c} - T_{i,c})/s_{se} = Q - W \tag{1.60}$$

1.1.4 Rankine power generation system

Based on different working fluids, there are two different kinds of Rankine power generation systems, steam Rankine power generation system and organic Rankine power generation.

1.1.4.1 Steam Rankine cycle

For steam Rankine cycle, a deaerator is used to remove the oxygen and other non-condensable gases in the feedwater of steam generating system. Dissolved oxygen in feedwater will cause serious corrosion damage in steam generating system by forming oxides (rust) of the metal pipes. Dissolved carbon dioxide combines with water to form carbonic acid will cause further corrosion. The accumulation of the non-condensable gases will increase the heat transfer resistance, which is harmful for the heat exchangers. The extraction of the steam turbine provides heat for the deaerator.

Figure 1-6a shows the T-s diagram of the water circuit in the cascade system in Figure 1-11. Process $2a$-$2c$-$2b$ shows the heat process in the steam turbine (see Figure 1-6b). State point $2b$ and $i, 2b$ have the same pressure, state point $2c$ and $i, 2c$ have the same pressure. To simplify the inner process $2a$-$2c$-$2b$ of the turbine, same isentropic efficiency of steam turbine with different loads and in different stages is assumed, which means

$$\eta_{i,tb} = (h_{2a} - h_{2b})/(h_{2a} - h_{i,2b}) = (h_{2a} - h_{2c})/(h_{2a} - h_{i,2c}) \tag{1.61}$$

where $h_{i,2b}$ is determined by s_{2a} and p_c; $h_{i,2c}$ is determined by s_{2a} and p_e.

The output power of the steam turbine

$$P_{tb} = (1 - y)\,\dot{m}_2\,(h_{2a} - h_{2b}) + y\dot{m}_2\,(h_{2a} - h_{2c}) \tag{1.62}$$

Process $2b$-$2d$ shows the heat process in the condenser. The outlet water in the condenser is saturated water. The outlet temperature T_{2d} and outlet enthalpy h_{2d} are determined by the exhaust pressure of the turbine p_c. The released heat of the condenser

$$Q_{cd} = (1 - y)\dot{m}_2(h_{2b} - h_{2d}) \tag{1.63}$$

State points $2c$, $2f$ and $2g$ have the same pressure (p_e, 1 MPa). The water at the outlet of the deaerator is saturated fluid, its enthalpy is determined.

$$yh_{2c} + (1 - y)h_{2f} = h_{2g} \tag{1.64}$$

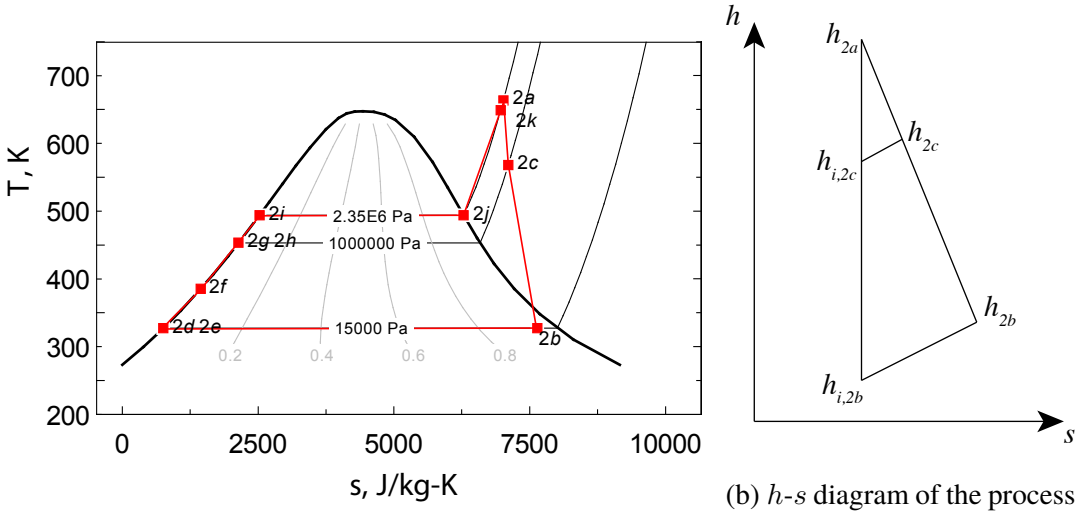

(a) T-s diagram of the water circuit

(b) h-s diagram of the process $2a$-$2c$-$2b$

图 1-6 T-s diagram of the water circuit and h-s diagram of the process $2a$-$2b$

The total power of the pumps

$$P_{pu} = (1-y)\,\dot{m}_2\,(h_{2e} - h_{2d}) + \dot{m}_2\,(h_{2h} - h_{2g}) \tag{1.65}$$

where h_{2e} can be obtained from $\eta_{pu} = (h_{i,2e} - h_{2d})/(h_{2e} - h_{2d})$, h_{2h} can be obtained from $\eta_{pu} = (h_{i,2h} - h_{2g})/(h_{2h} - h_{2g})$. $h_{i,2e}$ is determined by s_{2d} and p_e, $h_{i,2h}$ is determined by s_{2g} and p_s.

The outlet water of the deaerator is saturated water ($x = 0$), so the outlet temperature T_{2g} and outlet enthalpy h_{2g} of the heated fluid is determined by pressure p_{2g}. For the deaerator, the outlet pressure equals to any of the inlet pressure.

$$p_{2g} = p_{2c} \tag{1.66}$$

Heat injected in the water circuit

$$Q_2 = (1-y)\,\dot{m}_2\,(h_{2f} - h_{2e}) + \dot{m}_2\,(h_{2a} - h_{2h}) \tag{1.67}$$

The efficiency of Rankine cycle can be expressed as

$$\eta_{rk} = (P_{tb} - P_{pu}/\eta_{ge})/Q_2 \tag{1.68}$$

1.1.4.2 Organic Rankine cycle

Compared with steam Rankine cycle, ORC has the following features:

(1) Organic fluid has lower boiling point, and higher evaporation pressure. It is suitable for the recovery of low temperature waste heat. Besides, it has small density and specific heat capacity, the required size of turbine, pipes and heat transfer areas are small, which is beneficial for cost saving.
(2) The exhaust fluid of the turbine is dry. So without overheat, the saturated gas can be used as the main gas for the turbine. The corrosion situation caused by the impact of the droplets to the high-speed rotating blades will not happen with ORC.
(3) Organic fluid has lower sound speed than vapor, the turbine can achieve favorable aerodynamic performance with lower wheel speed.
(4) Organic fluid has higher condensing pressure than water. It can condense under the pressure higher than the atmosphere. The system pressure can be maintained above the atmosphere pressure to prevent air leak into the system. This means a deaerator is no more necessary.
(5) Organic fluid has low freezing point, no anti-freezing treatment is required even in the cold area.

The shapes of curves in the T-s diagram of different fluids are different. According to the saturated vapor curve dT/ds in the T-s diagram, the working fluid can be divided into three types: $dT/ds > 0$ means dry fluid (moisture does not form when high-pressure saturated vapor expanded reversibly from a high pressure) , most of the organic fluid are dry fluids; $dT/ds < 0$ means wet fluid (moisture forms when high-pressure saturated vapor expanded reversibly from a high pressure), such as water; $dT/ds \to \pm\infty$ means isentropic fluid, such as R134a. For the high temperature high pressure dry fluid and isentropic fluid, since there is no droplets after work in the expansion turbine, no superheater is required. On the other hand, since the purpose of the ORC focuses on the recovery of low grade heat power, a superheated approach like the traditional Rankine cycle is not appropriate.

Figure 1-7 shows the T-s diagram of steam Rankine cycle and ORC cycle. Figure 1-8 shows the schematic diagram of the ORC system. For a dry fluid, the cycle can be improved by the use of a regenerator: since the fluid has not reached the two-phase state at the end of the expansion, its temperature at this point is higher than the condensing temperature. This

higher temperature fluid can be used to preheat the liquid before it enters the evaporator. A counter-current heat exchanger is thus installed between the expander outlet and the evaporator inlet. The power required from the heat source is therefore reduced and the efficiency is increased.

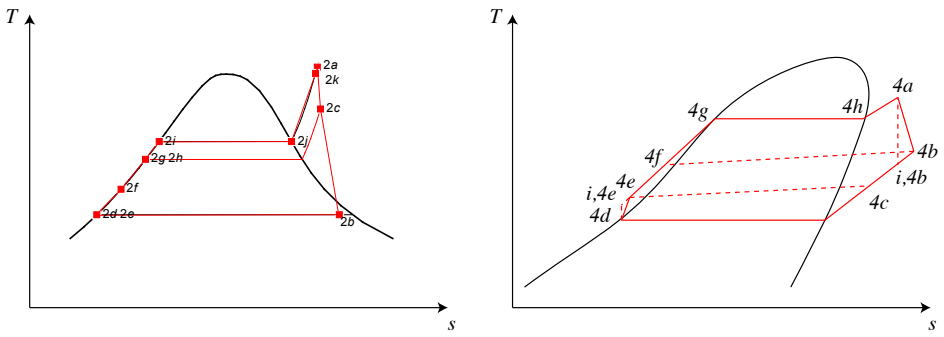

图 1-7 T-s diagram of water and a typical organic fluid in Rankine cycles

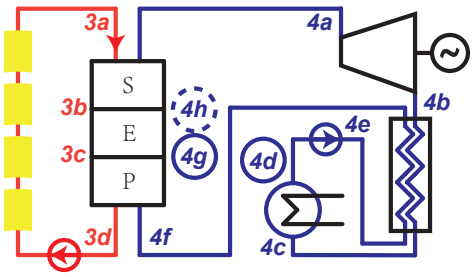

图 1-8 The schematic diagram of an ORC system with regenerator

The isentropic efficiency of the turbine

$$\eta_{i,tb} = (h_{4a} - h_{4b})/(h_{4a} - h_{i,4b}) \tag{1.69}$$

where $h_{i,4b}$ is determined by s_{4a} and p_c.

The output power of the turbine

$$P_{tb} = \dot{m}_4(h_{4a} - h_{4b}) \tag{1.70}$$

Process $4c$-$4d$ shows the heat process in the condenser. The outlet fluid of the condenser is saturated liquid. The outlet temperature T_{4d} and outlet enthalpy h_{4d} are determined by the exhaust pressure of the turbine p_c.

For the regenerator,

$$h_{4b} - h_{4c} = h_{4f} - h_{4e} \tag{1.71}$$

The released heat of the condenser

$$Q_{cd} = \dot{m}_4(h_{4c} - h_{4d}) \tag{1.72}$$

The power of the pump

$$P_{pu} = \dot{m}_4(h_{4e} - h_{4d}) \tag{1.73}$$

where h_{4e} can be obtained from $\eta_{pu} = (h_{i,4e} - h_{4d})/(h_{4e} - h_{4d})$. $h_{i,4e}$ is determined by s_{4d} and p_s.

Heat injected in the circuit

$$Q_4 = \dot{m}_4(h_{4a} - h_{4f}) \tag{1.74}$$

The efficiency of Rankine cycle can be expressed as

$$\eta_{rk} = \frac{P_{tb} - P_{pu}/\eta_{ge}}{\dot{m}_4(h_{4a} - h_{4f})} \tag{1.75}$$

1.1.4.3 Generator

The generator is relatively independent of the cascade system and its efficiency is assumed to be a constant value, 0.975.

1.2 Stirling engine array modeling

Stirling engine array is used in the cascade system, Figure 1-9 shows the layout of a Stirling engine array. Each Stirling engine in the Stirling engine array has the identical parameters: $U_{se,1} = 30\,\mathrm{W/(m^2 \cdot K)}$, $U_{se,2} = 150\,\mathrm{W/(m^2 \cdot K)}$, $A_{se,1} = 6\,\mathrm{m^2}$, $A_{se,2} = 6\,\mathrm{m^2}$, $k_{se} = 1.4$, $\gamma_{se} = 3.375$, $n_g = 7.84 \times 10^{-2}\,\mathrm{mol}$, $s_{se} = 10\,\mathrm{s^{-1}}$.

Depending on the direction of heating and cooling flows, there are two possible flow types: parallel flow and counterflow. Figure 1-10 and Figure 1-10b show the heat transfer diagrams of the two flow types. n_1 is chosen to be 10 and can be optimized later.

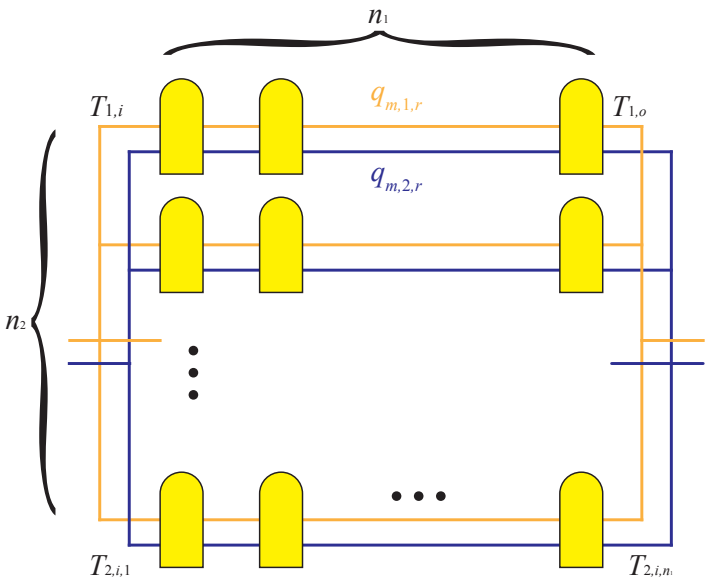

图 1-9　Layout of Stirling engines

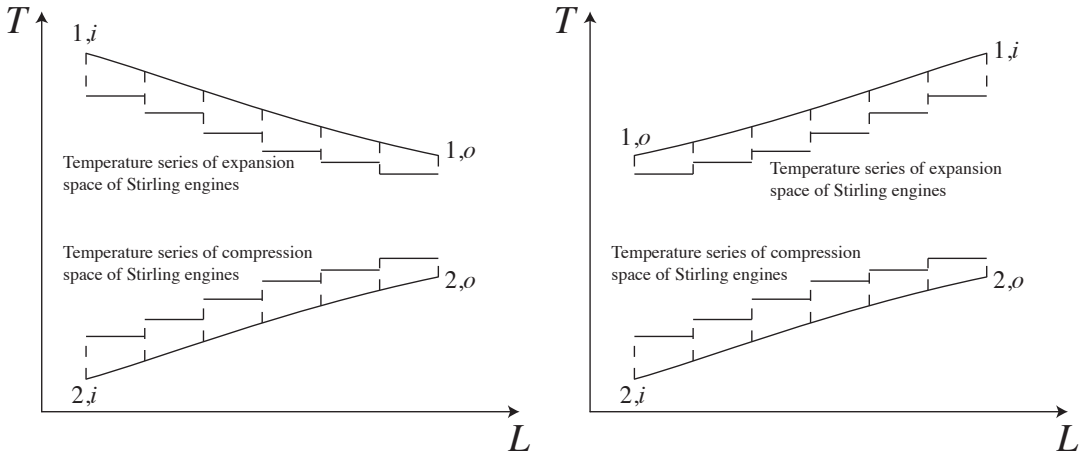

(a) Parallel flow　　(b) Counterflow

图 1-10　Heat transfer diagrams of parallel flow and counterflow

In Figure 1-9, $T_{1,i,1} = T_{1,i}, \dot{m}_{1,r} = \dot{m}_1/n_2$. For x from 1 to $n_1 - 1$, where x is the column number of Stirling engines, $T_{1,i,x+1} = T_{1,o,x}, T_{2,i,x+1} = T_{2,o,x}$.

Assume that the positive flow direction is to the right, for parallel flow, $T_{2,i,1} = T_{2,i}$, $\dot{m}_{2,r} = \dot{m}_2/n_2$; for counterflow, $T_{2,o,n_1} = T_{2,i}$, $\dot{m}_{2,r} = -\dot{m}_2/n_2$.

Assume linear temperature profile across the regenerator, the mean effective temperature $T_{R,x} = \dfrac{T_{H,x} - T_{L,x}}{\ln(T_{H,x}/T_{L,x})}$,[23,24] and the symmetrical regenerator behaviour assumption $e_x = \dfrac{T_{R,x} - T_{L,x}}{T_{H,x} - T_{L,x}}$.[15,16]

For a Stirling engine in column x, x from 1 to n_1, according to Equation (1.38) and Equation (1.39),

$$T_{hw,x} = T_{1,i,x} - \frac{T_{1,i,x} - T_{1,o,x}}{1 - \exp(-\dfrac{U_{se,1}A_{se,1}}{\dot{m}_{1,r}c_{p,1,x}})} \tag{1.76}$$

$$T_{cw,x} = T_{2,i,x} - \frac{T_{2,i,x} - T_{2,o,x}}{1 - \exp(-\dfrac{U_{se,2}A_{se,2}}{\dot{m}_{2,r}c_{p,2,x}})} \tag{1.77}$$

The power of each Stirling engine in column x can be written as

$$P_{se,x} = W_{th,x} - W_{pd,x} - W_{fs,x} \tag{1.78}$$

The efficiency of each Stirling engine in column x can be written as

$$\eta_{se,x} = \frac{W_{th,x} - W_{pd,x} - W_{fs,x}}{Q_{th,x} + Q_{id,x} + Q_{sc,x}} \tag{1.79}$$

For energy balance,

$$\dot{m}_{1,r}(h_{1,i,x} - h_{1,o,x})(1 - \eta_{se,x}) = \dot{m}_{2,r}(h_{2,o,x} - h_{2,i,x}) \tag{1.80}$$

Using equations in Section 1.1.3 and the energy balance equations, key parameters of the Stirling engine array can be obtained.

The efficiency of the Stirling engine array

$$\eta_{sea} = 1 - \frac{\dot{m}_2(h_{2,o,n_1} - h_{2,i,1})}{\dot{m}_1(h_{1,i,1} - h_{1,o,n_1})} \tag{1.81}$$

The output power of each Stirling engine in column x

$$P_{se,x} = \dot{m}_{1,r}(h_{1,i,x} - h_{1,o,x})\eta_{se,x} \tag{1.82}$$

The total output power of the Stirling engine array

$$P_{sea} = \eta_{sea}\dot{m}_1(h_{1,i,1} - h_{1,o,n_1}) \tag{1.83}$$

1.3 Steam generating system modeling

The steam generating system can be divided into preheater, evaporator and superheater, they are collectively referred to as PES. They are all heat exchangers. It is assumed that, in these heat exchangers, the pressure of the fluid does not change significantly. It can be assumed that the water pressure in the steam generating system equals to the pressure of the inlet pressure of the turbine. Besides, these heat exchangers do not exchange heat with the environment. To clearly understand the modeling process of these heat exchangers, an example of steam generating system as shown in Figure 1-11 is used for explanation. Figure 1-12 shows the T-Q diagram of the heat transfer process. State points of different fluids are marked on the sketch. The number indicates the type of the fluid, the letter indicates the state point of the fluid. A state point with solid circle indicates saturated liquid state ($x = 0$), and with dotted circle indicates saturated gas state ($x = 1$).

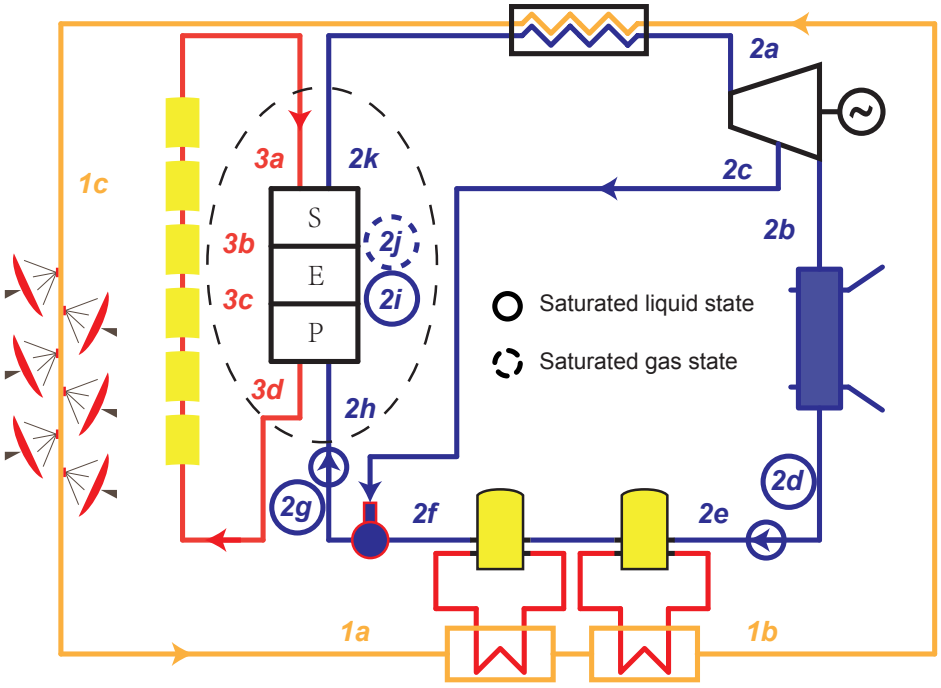

图 1-11 An example of steam generating system in a cascade system

The modeling process of PES is the process of solving the unknown states of the state

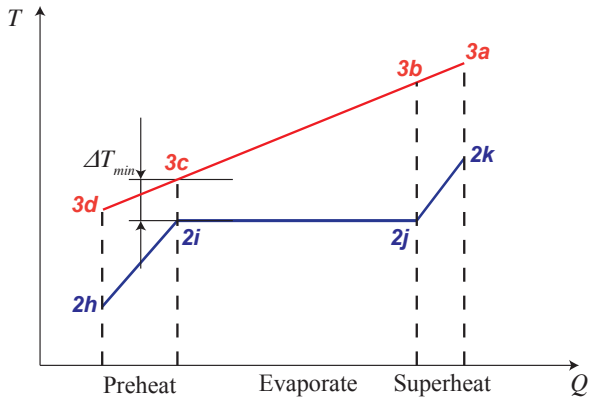

图 1-12　The steam generating process

points. Notice that, the pressure of the fluids keeps constant in the heat transfer process. For an unsaturated state, known the temperature or enthalpy, the state is determined. This means, the temperature can be obtained from the enthalpy, and vice versa. For a saturated state, known the dryness (x) of the fluid, the state is determined.

For a typical PES modeling process as shown in Figure 1-11, $\dot{m}_2$, state $2h$ and state $2k$ are determined by the parameters of the turbine. State $3a$ is determined by the design parameters. State $2i$ and state $2j$ are determined by their dryness values.

(1) *Preheater*

The outlet of the heated fluid is saturated liquid ($x = 0$), so the outlet temperature T_{2i} and outlet enthalpy h_{2i} of the heated fluid are determined by the main pressure of the turbine, p_s.

$$\dot{m}_3(h_{3c} - h_{3d}) = \dot{m}_2(h_{2i} - h_{2h}) \tag{1.84}$$

(2) *Evaporator*

The outlet of the heated fluid is saturated gas ($x = 1$), so the outlet temperature T_{2j} and outlet enthalpy h_{2j} of the heated fluid are determined by the main pressure of the turbine, p_s.

$$\dot{m}_3(h_{3b} - h_{3c}) = \dot{m}_2(h_{2j} - h_{2i}) \tag{1.85}$$

It has to be mentioned that, state $3c$ is determined by T_{3c}, which equals to $T_{2i} + \Delta T_{min}$. ($T_{3c} = T_{2i} + \Delta T_{min}$)

(3) *Superheater*

For the energy balance,

$$\dot{m}_3(h_{3a} - h_{3b}) = \dot{m}_2(h_{2k} - h_{2j}) \tag{1.86}$$

By solving the equations (1.84) to (1.86), $\dot{m}_3$, state $3b$ and $3d$ can be obtained.

1.4 System modeling

Different components are connected to form a system by their interfaces (inlets and outlets). These interfaces are interacted with each other by "streams". For example, the steam turbine in Figure 1-11 is connected with the deaerator by a steam stream. This steam stream has its own properties such as fluid type, mass flow rate, temperature, pressure and so on. "Steams" are defined as objects in the modeling language – MATLAB. Appendix C shows the source code of the definition of the class – **Stream**.

Some properties, **T**, **q_m** and **p**, of **Stream** are also objects. They belong to the classes **Temperature**, **Massflow** and **Pressure** separately.

Given the inherent properties of a **Stream**, its dependent properties, mass specific enthalpy (**h**), mass specific entropy (**s**) and pressure (**p**), can be obtained.

If the stream is a single phase stream, its dryness does not exist. Its dependent properties (h, s, c_p) can be obtained from its temperature (T) and pressure (p) by calling the open source MATALB wrapper CoolProp. If the stream is a two-phase stream, $0 \leqslant x \leqslant 1$. Its dependent properties (h, s, c_p) can be obtained from its pressure (p) and dryness (x). The reason of choosing pressure (p) instead of temperature (T) as the input value is that it is easier to be determined.

A **stream** can be used to record a state point since it contains all the information for a state point. Streams are defined in a system for component connection and system calculation. Different components are connected by streams to form a system. The Streams are passed as parameters to the components, completing the calculation of the methods in the components.

Components are connected each other by streams. Their inlets and outlets are used as interfaces for connection. Two interfaces are connected together by being assigned the same stream.

Systems are initialized by given parameters (design parameters). These parameters are assigned to corresponding properties of the streams and thus affect the state of the related components.

For system calculation, it has to be mentioned that, some parameters of a component are related with other components. In such situations, guess values are used for the calculation methods in the components. The guess values are set to be the properties of some streams. Each of these streams is assigned to two components (evaporator and superheater). These streams are assigned to corresponding components to accomplish the calculation methods in the components. These calculation methods will return solutions for the stream parameters. Then the parameters will be compared with the guess values for verification. If the differences between guess values and the calculated parameters are within permissible error, the guess values are accepted; otherwise, the guess values will be iteratively readjusted according to the Runge-Kutta method until accepted.

For example, the mass flow rate of oil of the evaporator ($\dot{m}_3$) is related with the superheater in a system as described in Figure **??**. A guess value of $\dot{m}_3$, $\dot{m}_{3,g}$, is required to determine it. $\dot{m}_{3,g}$ is assigned to the evaporator oil stream. This stream is assigned to both evaporator and superheater. In **evaporator**, the method **get_T_3b** will change the temperature of the stream (T_{3b}) from the default value. In **superheater**, the method **get_q_m_3** will return a solution of $\dot{m}_3$, $\dot{m}_{3,s}$, for verification. If $|\dot{m}_{3,g} - \dot{m}_{3,s}|$ is less than permissible error (10^{-4}), then $\dot{m}_{3,g}$ is accepted as the value of $\dot{m}_3$; otherwise, $\dot{m}_{3,g}$ will be iteratively readjusted according to the Runge-Kutta method until $|\dot{m}_{3,g} - \dot{m}_{3,s}| < 10^{-4}$.

1.5 Conclusion

This chapter presents the modeling method of the cascade system and introduces the modeling of some key components and subsystems in detail. The component models are developed in MATLAB using object-oriented method. Bottom-up design method is applied for system development. Models of the components of a system are developed first according to their mechanism characteristics, and the system model is established by these component models. A MATLAB class **Stream** created for component connection is used as an example to introduce the system modeling process. The components' inlets and outlets are used as interfaces for connection. Two interfaces are connected together by being assigned the same stream. The calculation process related with different components is also briefly introduced in this chapter.

Due to the encapsulation, composition and polymorphism of the object-oriented language, the system model has some advantages such as easy to establish, convenient to replace

a component and clearly check the performance of specific components.

The key component models in the cascade system can be validated experimentally or be compared with the classic models. The validation of Stirling engine model shows that the proposed model has much better agreement with the experimental results than previous classic thermal models at various rotation speeds and mean effective pressures.

参考文献

[1] Babaelahi M, Sayyaadi H. A new thermal model based on polytropic numerical simulation of Stirling engines. Applied Energy, 2015, 141:143 – 159.

[2] MARTINI W R. Stirling engine design manual, 2nd edition. Technical report, Martini Engineering, Richland, WA (USA), 1983.

[3] Price H, Lupfert E, Kearney D, et al. Advances in Parabolic Trough Solar Power Technology. Journal of Solar Energy Engineering, 2002, 124(2):109–125.

[4] Dudley V E, Kolb G J, Mahoney A R, et al. Test results: SEGS LS-2 solar collector. Nasa Sti/recon Technical Report N, 1994, 96(4):2506–2514.

[5] Romero-Alvarez M, Zarza E. Concentrating solar thermal power. Efficiency and Renewable Energy, 2007.

[6] Adkins D R. Control strategies and hardware used in solar thermal applications. Nasa Sti/recon Technical Report N, 1987, 88.

[7] Coronel P, Sandeep K. Heat transfer coefficient in helical heat exchangers under turbulent flow conditions. International Journal of Food Engineering, 2008, 4(1).

[8] Serth R W. Process heat transfer principles and applications. Amsterdam; London: Elsevier Academic Press, 2007.

[9] Churchill S W, Bernstein M. A Correlating Equation for Forced Convection From Gases and Liquids to a Circular Cylinder in Crossflow. Journal of Heat Transfer, 1977, 99(2):300–306.

[10] Ma R Y. Wind Effects on Convective Heat Loss From a Cavity Receiver for a Parabolic Concentrating Solar Collector. Sandia National Laboratory, 1993, SAND92-7293(September).

[11] Wu S Y, Xiao L, Cao Y, et al. Convection heat loss from cavity receiver in parabolic dish solar thermal power system: A review. Solar Energy, 2010, 84(8):1342 – 1355.

[12] Leibfried U, Ortjohann J. Convective Heat Loss from Upward and Downward-Facing Cavity Solar Receivers: Measurements and Calculations. Journal of Solar Energy Engineering, 1995, 117(2):75–84.

[13] Koenig A, Marvin M. Convection heat loss sensitivity in open cavity solar receivers. Technical report, Department of Energy, USA, 1981.

[14] Stine W B, Diver R B. A compendium of solar dish/Stirling technology. Technical report, DTIC Document, 1994.

[15] Formosa F, Despesse G. Analytical model for Stirling cycle machine design. Energy Conversion and Management, 2010, 51(10):1855–1863.

[16] Juhasz A. A mass computation model for lightweight brayton cycle regenerator heat exchangers. in: Proceedings of 8th Annual International Energy Conversion Engineering Conference, 2010.

[17] Duan C, Wang X, Shu S, et al. Thermodynamic design of Stirling engine using multi-objective particle swarm optimization algorithm. Energy Conversion & Management, 2014, 84:88–96.

[18] Urieli I, Berchowitz D M. Stirling cycle engine analysis. Bristol: A. Hilger, 1984.

[19] Heywood, JohnB. Internal combustion engine fundamentals. Amsterdam; London: McGraw-Hill, 1988.

[20] Strauss J M, Dobson R T. Evaluation of a second order simulation for Sterling engine design and optimisation. Journal of Energy in Southern Africa, 2010, 21(2):17–29.

[21] Timoumi Y, Tlili I, Nasrallah S B. Design and performance optimization of GPU-3 Stirling engines. Energy, 2008, 33(7):1100 – 1114.

[22] Hosseinzade H, Sayyaadi H, Babaelahi M. A new closed-form analytical thermal model for simulating Stirling engines based on polytropic-finite speed thermodynamics. Energy Conversion and Management, 2015, 90:395 – 408.

[23] Der Minassians A. Stirling Engines for Low-temperature Solar-thermal-electric Power Generation: [PhD Dissertation]. Berkeley: EECS Department, University of California, Berkeley, December 20, 2007.

[24] Cavazzuti M. Optimization Methods: From Theory to Design Scientific and Technological Aspects in Mechanics. Berlin Heidelberg: Springer, 2012.

附录 A　Heat transfer under constant temperature

Assuming U, T_c, $\dot{m}$,c_p to be constant, for given T_i,

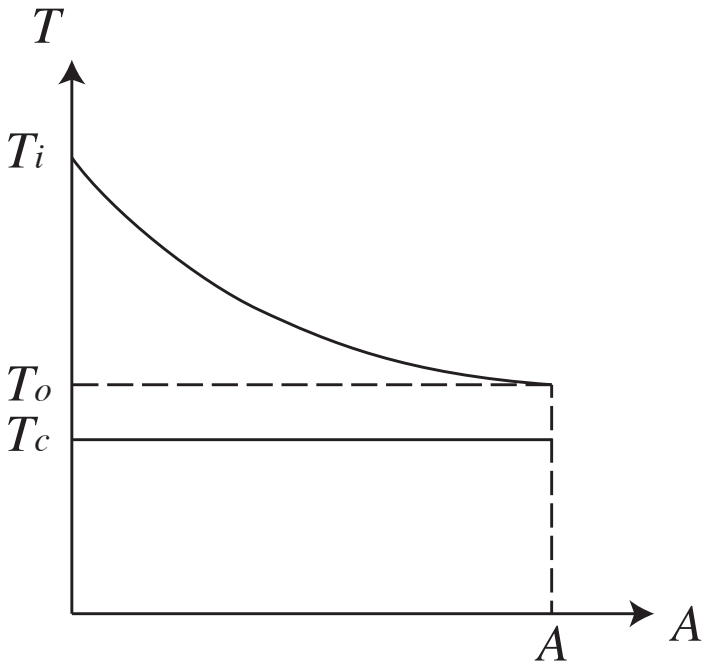

图 1-1　Diagram of heat transfer under constant temperature

For $A(x) = Px$, x from 0 to L, while $T(x)$ from T_i to T_o,

$$\dot{m}c_p dT(x) = (T_c - T(x))UPdx \tag{A.1}$$

so

$$\frac{dT(x)}{dx} = -\frac{UP}{\dot{m}c_p}(T(x) - T_c) \tag{A.2}$$

$$T_g(x) = T_p(x) + T_h(x) \tag{A.3}$$

where $T_g(x)$ is the general solution, $T_p(x)$ is the particular solution, $T_h(x)$ is the homogeneous solution.

$$-\frac{UP}{\dot{m}c_p}(T_p(x) - T_c) = 0 \tag{A.4}$$

$$T_p(x) = T_c \tag{A.5}$$

$$\frac{dT_h(x)}{dx} = -\frac{UP}{\dot{m}c_p}T_h(x) \tag{A.6}$$

$$\int_{T_h(x)=T_h(0)}^{T_h(x)=T_h(L)} \frac{dT_h(x)}{T_h(x)} = -\int_{x=0}^{x=L} \frac{UP}{\dot{m}c_p}dx \tag{A.7}$$

$$\frac{T_h(L)}{T_h(0)} = \exp(-\frac{UPL}{\dot{m}c_p}) \tag{A.8}$$

that is

$$\frac{T_g(L) - T_p(L)}{T_g(0) - T_p(0)} = \exp(-\frac{UA}{\dot{m}c_p}) \tag{A.9}$$

$$\frac{T_o - T_c}{T_i - T_c} = \exp(-\frac{UA}{\dot{m}c_p}) \tag{A.10}$$

附录 B　Thermal gradient under constant heat flux

Assuming U, T_c, $\dot{m}$, c_p, q'' to be constant, for given T_i,

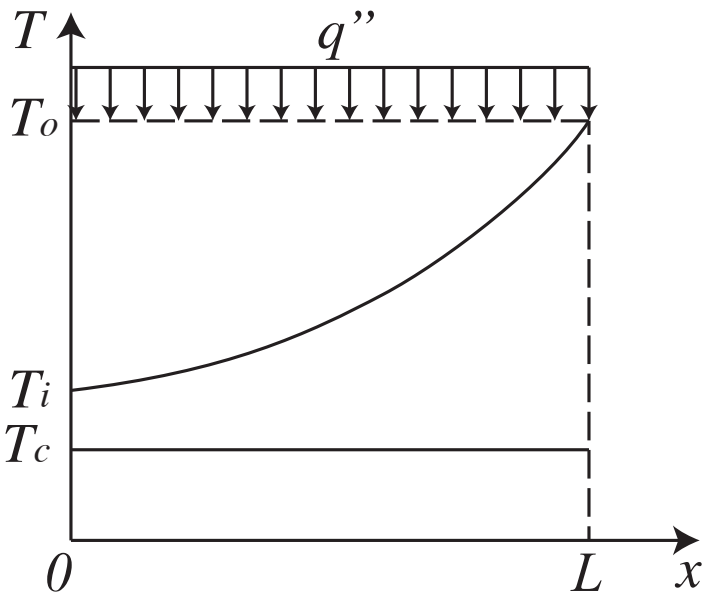

图 2-1　Diagram of heat transfer with one constant temperature heat source and constant heat flux

For $A(x) = Px$, x from 0 to L, while $T(x)$ from T_i to T_o,

$$\dot{m}c_p dT(x) = (T_c - T(x))UPdx + q''Pdx \tag{B.1}$$

so

$$\frac{dT(x)}{dx} = -\frac{UP}{\dot{m}c_p}T(x) + \frac{q''P + UPT_c}{\dot{m}c_p} \tag{B.2}$$

$$T_g(x) = T_p(x) + T_h(x) \tag{B.3}$$

where $T_g(x)$ is the general solution, $T_p(x)$ is the particular solution, $T_h(x)$ is the homogeneous solution.

$$-\frac{UP}{\dot{m}c_p}T_p(x) + \frac{q''P + UPT_c}{\dot{m}c_p} = 0 \tag{B.4}$$

$$T_p(x) = T_c + \frac{q''}{U} \tag{B.5}$$

$$\frac{dT_h(x)}{dx} = -\frac{UP}{\dot{m}c_p}T_h(x) \tag{B.6}$$

the same as Equation (A.6), so we have

$$\frac{T_g(L) - T_p(L)}{T_g(0) - T_p(0)} = \exp(-\frac{UA}{\dot{m}c_p}) \tag{B.7}$$

$$\frac{T_o - T_c - \dfrac{q''}{U}}{T_i - T_c - \dfrac{q''}{U}} = \exp(-\frac{UA}{\dot{m}c_p}) \tag{B.8}$$

附录 C　MATLAB code of class Stream

```
classdef Stream < handle
    %Stream This class describes a fluid stream that has inherent
    %properties and dependent properties

    properties
        fluid;  % Fluid type
        dot_m;  % Mass flow rate, kg/s
        T;      % Temperature, K
        p;      % Pressure, Pa
        x;      % Quality, [0, 1] for two phase stream; NaN for single
                %   phase stream
    end
    properties(Dependent)
        h;      % Mass specific enthalpy, J.kg
        s;      % Mass specific entropy, J/kg-K
        cp;     % Specific heat under constant pressure, J/kg-K
    end

    methods
        function obj = Stream
            obj.T = Temperature;
            obj.dot_m = Massflow;
            obj.p = Pressure;
        end
        function flowTo(obj, st)
            st.fluid = obj.fluid;
            st.dot_m = obj.dot_m;
        end
        function st2 = mix(obj, st1)
            % Get the properties of a stream mixed by two streams
            % The two streams must have the same fluid type and pressure
            if obj.fluid == st1.fluid
                if  obj.p.v == st1.p.v
                    obj.p = st1.p;
                    st2.fluid = obj.fluid;
                    st2.p = obj.p;
                    st2.dot_m.v = obj.dot_m.v + st1.dot_m.v;
                    h = (obj.dot_m.v .* obj.h + st1.dot_m.v .* st1.h)...
                        ./ (obj.dot_m.v + st1.dot_m.v);
                    st2.T.v = CoolProp.PropsSI('T', 'H', h, 'P',st2.p.v);
                else
                    error('The two streams have different pressures!');
                end
            else
```

```
                error('The two streams have different fluid types!');
            end
        end
        function convergeTo(obj, st, y)
            % Get another stream converged (or diverged)
            % from the original stream state.
            % If y < 1, the original stream is diverged
            % If y > 1, the original stream is converged
            st.fluid = obj.fluid;
            st.T = obj.T;
            st.p = obj.p;
            st.x = obj.x;
            st.dot_m.v = obj.dot_m.v .* y;
        end
    end
    methods
        % The dependent properties can be obtained from the inherent
        %   properties
        % If x is NaN, then the dependent properties are determined
        %   by T and P; otherwise, they are determined by P and x
        function value = get.h(obj)
            if isempty(obj.x)
                value = CoolProp.PropsSI('H', 'T', obj.T.v, ...
                    'P', obj.p.v, obj.fluid);
            else
                value = CoolProp.PropsSI('H', 'P', obj.p.v, 'Q', ...
                    obj.x, obj.fluid);
            end
        end
        function value = get.s(obj)
            if isempty(obj.x)
                value = CoolProp.PropsSI('S', 'T', obj.T.v, ...
                    'P', obj.p.v, obj.fluid);
            else
                value = CoolProp.PropsSI('S', 'P', obj.p.v, 'Q', ...
                    obj.x, obj.fluid);
            end
        end
        function value = get.cp(obj)
            if isempty(obj.x)
                value = CoolProp.PropsSI('C', 'T', obj.T.v, ...
                    'P', obj.p.v, obj.fluid);
            else
                value = inf;
            end
        end
    end
end
```

附录D　攻读学位期间发表的学术论文

[1] Cheng Zhang, Yanping Zhang, Inmaculada Arauzo, Wei Gao, Chongzhe Zou. Cascade system using both trough system and dish system for power generation. Energy Conversion and Management. 2017.06.15;142:494–503.

[2] Cheng Zhang, Yanping Zhang, Xiaolin Lei, Wei Gao. Design and Comparison of Solar Thermal Oilfield Steam Production System Plans. Journal of Solar Energy Engineering. 2017.01.08;139;004502-4.

[3] Cheng Zhang, Kun Wang, Jizhou Wang, Shuhong Huang. FEA simulation on the alignment of the shafts of three-fulcrum turbine. International Conference on Power Engineering. 2013.

[4] Chongzhe Zou, Yanping Zhang, Quentin Falcoz, Pierre Neveu, Cheng Zhang, Shuhong Huang, Weicheng Shu. Design and Optimization of a High-temperature Cavity Receiver for a Solar Energy Cascade Utilization System. Renewable Energy. 2017.04.01:103; 478-89.

[5] Chongzhe Zou, Yanping Zhang, Huayi Feng, Quentin Falcoz, Pierre Neveu, Cheng Zhang, Wei Gao. “Effects of Geometrical Parameters on Thermal Performance for a Cylindrical Solar Receiver Using 3D numerical Model.” Energy Conversion and Management, 2017.10.1: 126-17.

[6] Chongzhe Zou, Yanping Zhang, Quentin Falcoz, Pierre Neveu , Cheng Zhang. Thermal modeling of a pressurized air cavity receiver for solar dish Stirling system, Solarpaces: International Conference on Concentrating Solar Power & Chemical Energy Systems. AIP Publishing LLC, 2017:1884-1892.

[7] A solar thermal cascade system, No. 201610806296.5

[8] A flow control method used in a multistage heating system, No. 201610805604.2